

## Integrative and Comparative Biology

# The Importance of a Filament-like Structure in Aerial Dispersal and the Rarefaction Effect of Air Molecules on a Nanoscale Fiber: Detailed Physics in Spiders' Ballooning

Journal:	Integrative and Comparative Biology
Manuscript ID	ICB-2020-0063.R1
Manuscript Type:	Symposium article
Date Submitted by the Author:	21-May-2020
Complete List of Authors:	Cho, Moonsung; Technical University of Berlin, Chair of Bioprocess Engineering, Institute of Biotechnology; University of Rostock, Department of Animal Physiology Santibáñez Koref, Iván; Bionics and Evolution Technique
Keywords:	spider, ballooning flight, animal locomotion, Low-Reynolds-number flows, Knudsen number, Rarefied gas dynamics

SCHOLARONE™ Manuscripts The Importance of a Filament-like Structure in Aerial Dispersal and

the Rarefaction Effect of Air Molecules on a Nanoscale Fiber:

Detailed Physics in Spiders' Ballooning

Moonsung Cho, 1,2,\* and Iván Santibáñez Koref 3

- (1) Technical University of Berlin, Institute of Biotechnology, Ackerstraße 76 / ACK 24, 13355 Berlin, Germany
- (2) University of Rostock, Animal Physiology, Albert-Einstein-Str. 3, 18059 Rostock, Germany
- (3) Bionics and Evolution Technique, Ackerstraße 76 / ACK 1, 13355 Berlin, Germany

\*Author for correspondence, E-mail: moonsung.cho@uni-rostock.de

Many flying insects utilize a membranous structure for flight, which is known as a "wing." However, some spiders use silk fibers for their aerial dispersal. It is well known that spiders can disperse over hundreds of kilometers and rise several kilometers above the ground in this way. However, little is known about the ballooning mechanisms of spiders, owing to the lack of quantitative data. Recently, Cho et al. discovered previously unknown information on the types and physical properties of spiders' ballooning silks. According to the data, a crab spider weighing 20 mg spins 50–60 ballooning silks simultaneously, which are about 200 nm thick and 3.22 m long for their flight. Based on these physical dimensions of ballooning silks, the significance of these filament-like structures is explained by a theoretical analysis reviewing the fluid-dynamics of an anisotropic particle (like a filament or a high-slender body). (i) The filament-like structure is materially efficient geometry to produce (or harvest, in the case of passive flight) fluid-dynamic force in a low Reynolds number flow regime. (ii) Multiple nanoscale fibers are the result of the physical characteristics of a thin fiber, the drag of which is proportional to its length but not to its diameter. Because of this nonlinear characteristic of a fiber, spinning multiple thin ballooning fibers is, for

spiders, a better way to produce drag forces than spinning a single thick spider silk, because spiders can maximize their drag on the ballooning fibers using the same amount of silk dope. (iii) The mean thickness of fibers, 200 nm, is constrained by the mechanical strength of the ballooning fibers and the rarefaction effect of air molecules on a nanoscale fiber, because the slip condition on a fiber could predominate if the thickness of the fiber becomes thinner than 100 nm.

**Keywords:** spider, ballooning, ballooning flight, animal locomotion, fiber, spider silk, low Reynolds number flow, Knudsen number, rarefied gas dynamics



## Introduction

It is well known that spiders can disperse aerially over hundreds of kilometers and as high as a few kilometers (Darwin 1845, Glick 1939, Cho et al. 2018, Morley and Robert 2018). Research attention has been drawn to this passive flight of spiders, which is known as "ballooning," for several reasons: (i) the utilization of external energy for aerial dispersal, (ii) little understanding of the underpinning physical mechanisms, and (iii) the geometric uniqueness of the physical traits (silk: a filament-like structure) (Lee et al. 2015, Zhao et al. 2017, Cho et al. 2018, Morley and Robert 2018).

While most flying insects utilize membranous structures for their aerial locomotion (Dudley and Robert 2002, Sane 2003, Bomphrey 2017), the physical trait that enables spiders' aerial dispersal is a filament-like structure. This interesting trait has been investigated historically from the viewpoint of fluid dynamics. Humphrey considered that spiders use a single dragline for their flight, assuming it to be a rigid, thin, circular cylinder. He constructed a possible flight envelope, defining fluid-dynamic and mechanical constraints. However, the research could not explain the flight of a spider which weighs more than 9 mg (Humphrey 1987). Later, the chaotic movement of air flows and turbulence in the atmosphere were suggested as the physical factor that serves to prolong its drafting duration in the air (Suter 1999). The importance of the unsteady air flow (turbulence) on a flexible spider silk is also raised by Zhao et al. (2017). However, because of the lack of knowledge about ballooning silks, quantitative analysis was not possible (Sheldon et al. 2015). Recently, Cho et al. identified the types of ballooning silks among seven various spider silks and the quantity of ballooning silks used during the initial spinning phase. Crab spiders 18 to 20 mg in weight spun two thick (an average of 722 nm, N=4) minor ampullate gland silks and 48 to 58 thin (an average of 211 nm, N=40) aciniform gland silks simultaneously for their flight (see Figure 1). The length of the ballooning fibers ranged from 1.2 to 6.1 m, the average being 3.22 m (N=22). The values of the physical properties of the ballooning silks enabled quantitative analysis, which showed that even 10–150 mg large spiders (small spiders: 0.5-10 mg) could be lifted off with the help of a light updraft, utilizing their tens of ballooning fibers. Besides fluid-dynamics, the role of Earth's vertical electric field has been also investigated (Gorham 2013, Morley and Robert 2018).

Figure 1 (A) A crab spider (*Xysticus* spp.) with ballooning fibers just before takeoff. (B) A picture of ballooning fibers by SEM (  $\times$  10,000). Two thick silks are the silks spun from minor ampullate silk glands. Multiples thin silks are aciniform silks. (Photos from Cho et al. 2018)

Most physical traits in animals and plants are believed to have been largely optimized during their long evolution but are still evolving with changes of the physical and ecological environments. Phenotypic similarities of wings and flippers among different species of animals could be representative examples (Hoelzel 2009, Alexander 2015). The geometry of the bird's wing itself (Wang and Clarke 2015), the microstructure of a shark's skin (Oeffner and Lauder 2012, Ferrón and Botella 2017) and the microscopic setae on gecko's feet (Autumn and Peattie 2002, Autumn et al. 2002) could be also other examples relating with animal locomotion. However, the physical benefits why spiders use such a physical trait for their aerial dispersal have not yet been investigated. Hence, we pose three questions here. First, why do spiders use a filament-like structure for their aerial dispersal? Are there any aerodynamic and biological advantages in such a geometric trait? Second, why do spiders use multiple ballooning fibers? Third, is there any mechanical or fluid-dynamic significance in the mean thickness of 200 nm ballooning fiber? These questions will be explored mathematically using Burgers' approximate solution.

## Fluid-Dynamic Characteristics of a Ballooning Silk

Based on Cho's observed data, a ballooning fiber experiences low Reynolds-number flow regimes at each microscopic segment because of its extreme thinness. The upper limit of the Reynolds number is approximately 0.04 ( $Re = \rho Ud/\mu$ ; air density: 1.225 kg m<sup>-3</sup>; maximum possible velocity: 3 m s<sup>-1</sup>; thickness of spider silk: 211 nm; dynamic viscosity of air: 1.837 x 10<sup>-5</sup> kg m<sup>-1</sup> s<sup>-1</sup>). Because of the high aspect ratio of a ballooning fiber,1.61 ×  $10^{7}$ , the fiber can be regarded as an extremely thin, circular cylinder.

An available filament model for fluid dynamics is developed by Burgers' solution, approximating the contour of an ellipsoid, which has the exact solution for external viscous fluid flow, to the more similar contour to a cylinder (Burgers 1938). Eqns. (1) and (2) shows the resistance forces of a slender cylindrical body in the normal direction

and tangential to the axis of the cylindrical body, respectively. These equations are frequently used for the investigation of the dynamics of an anisotropic particle or a fiber in low Reynolds-number flow (Childress 1981, Happel and Brenner 1986, Humphrey 1987, Fung 1990, Barth et al. 1991).

$$F_N = \frac{4\pi\mu UL}{ln\left(2\frac{L}{d}\right) + 0.5}\tag{1}$$

$$F_T = \frac{2\pi\mu UL}{\ln\left(2\frac{L}{d}\right) - 0.72} \tag{2}$$

The drag force in the direction normal to the axis of the cylinder,  $F_N$ , is about twice as large as that in the direction parallel to the axis,  $F_T$  (see Purcell 1977, Childress 1981, Happel and Brenner 1986). The plausibility of the equations can easily be checked by dropping straight and cylindrical steel wires of lengths 30–80 mm and thicknesses ranging from 0.3 to 0.8 mm into corn syrup with viscosities ranging from 2 to 3 kg/ms (a "drop test"). The drag forces of these steel wires are measured in both directions (transverse, in the direction perpendicular to the axis, and longitudinally, in the direction of the axis). Simulation results of the bead-spring model are additionally compared (Cho 2020). The non-dimensional resistance coefficients are defined for comparison (see Eqns. (3) and (4)). The theoretical values coincide very well with those of the experiments and the simulation values (see Figure 2).

$$R_N = \frac{F_N}{\mu U L} \tag{3}$$

$$R_T = \frac{F_T}{\mu U L} \tag{4}$$

Figure 2 (A) Dimensionless longitudinal (tangential) resistance coefficients of a thin cylinder as a function of the slenderness of the cylinder. (B) Dimensionless transverse (normal) resistance coefficients of a thin cylinder as a function of the slenderness of the cylinder. The red solid lines are theoretical values. The triangular markers are the calculated values from the simulation using the bead-spring model. The square markers are the values obtained from the drop test (Cho 2020).

The important fluid-dynamic characteristic of a high-aspect-ratio circular cylinder, a thin filament, is that the resistance (drag) force is proportional to its length but not to its diameter. The drag force on a fiber does not increase proportionally as the diameter increases. Conversely, the drag force on a fiber does not decrease proportionally as the diameter decreases. Even though the thickness of 1µm fiber reduces to 50% of its original size while maintaining its constant length, the drag force does not become 50% of its original drag but remains at 90% of it. This nonlinear characteristic is the essential factor for understanding the advantages of this filament trait in its aerial and hydrodynamic locomotion. Figure 3 shows these linear and nonlinear variations of the drag force of a thin fiber according to its diameter and length. Suter's empirical values (Eqns. (5)) are almost twice as large as the theoretical values (Eqn. (2)); however, the empirical values also show the linear and nonlinear variations of the drag force (Suter 1991, Cho et al. 2018). Suter's empirical formula (Eqn. (5)) is established based on the measurements of resistance force of a drag line among different sizes of spiders.

$$F_{T_{Suter}} = 11.5UL \frac{\pi (d \times 10^6)^2 + 0.184^{0.094}}{0.0277}$$
 (5)

Figure 3 (A) The variation of resistance (drag) force on a thin fiber, which is 1 meter long, according to its diameter. The fluid medium is air. The flow velocity is 1 m/s. (B) The variation of resistance (drag) force on a thin fiber, the diameter of which is 1  $\mu$ m, according to its length. The fluid medium is air. The flow velocity is 1 m/s. The red solid lines are theoretical values with respect to equations (1) and (2). The black dashed lines are empirical values that are calculated by Suter's formula (see Eqn. (5); Suter 1991, Cho et al. 2018).

### Why do Spiders Utilize a Filament-Like Structure?

While other comparable insects usually use their membranous structures (wings) to achieve flight (Dudley and Robert 2002, Sane 2003, Bomphrey 2017), spiders use filament-like structures for aerial dispersal (Cho et al. 2018). Such filament-like structures are usually found in micro-organisms ( $E.\ coli$ , paramecia, etc.) or cells (e.g., sperm) that actively locomote in a liquid medium. Because of the extreme thinness of their cilia and flagella, the flow condition around them is a Stokes regime (Re < 1), in which the viscosity of the fluid medium is far more dominant than its inertia. However, some plants and animals also use filament-like structures for their aerial

journey. Plumed seeds, such as those of the dandelion and thistle, use a pappus as a parachute for their passive dispersal (Green and Johnson 1990, Minami et al. 2003, Casseau et al. 2015, Cummins et al. 2017, 2018).

Why do all these micro-organisms, seeds, and cells utilize hairy structures for their locomotion or aerial dispersal? The characteristic of the low Reynolds-number flow gives us the answer. In a flow of this kind, where the viscosity of the fluid medium is dominant, the fluid-dynamic force is proportional to the size (length, neither area nor volume) of the object. Table 1 shows the fluid dynamic forces (resistance force) of various geometries, which represent one- to three-dimensional objects, respectively. The forces on those geometries in the low Reynoldsnumber flow are proportional to either a diameter ( $\propto \alpha$ : radius) for a sphere and a circular disk or a length L. which is the dominant length in the case of a fiber. On the other hand, the fluid dynamic force is proportional to the area ( $\propto a^2$ ) in cases of moderate and high Reynolds-number flows (Re > 1000). This is because the fluid dynamic force in a high Reynolds-number flow is proportional to the dynamic pressure of the fluid flow, which acts on the surface of an object. However, the weight of each geometry, which is proportional to its volume, increases in proportion to  $a^3$  for a sphere,  $a^2$  for a disk, and L for a thin, cylindrical rod, respectively. For living animals, the important point is how much protein they invest to construct a certain physical trait and how much they achieve the desired functionality. The ratio of a drag force to a weight represents the cost efficiency, which means how much fluid dynamic force is gained by investing a certain amount of physical material (see Eqn. (6)). While the cost efficiencies of a sphere and a disk decrease as the size increases, the cost efficiency of a thin rod stays constant, independently of its size. If we apply the same analysis to the objects in the moderate/high Reynolds-number flow, the cost efficiency of a disk shows independence of its size (see Table 1). This is why the micro-organisms that swim in a viscous environment use cilia and flagella and why macro-insects over a few milligrams in weight tend to use membranous structures for their flight, because they utilize the moderate and high Reynolds-number flows (Re > 1000). This is the same in the case of birds and airplanes, the Reynolds numbers of which are in the range of  $10^3$  to  $10^7$  (Lissaman 1983). The filament-like structures are also found in passive flyers as the morphological structures of pappus, stiff setae, and spider silks. In conclusion, the filamentlike structure is regarded as a materially efficient structure to produce fluid dynamic forces (mostly a viscous force) in the low Reynolds-number flow. The interesting point to note here is that a spider is the heaviest organism that uses fiber structures for its flight, some species exceeding tens of milligrams in weight. This is possible because spiders can spin extremely thin, strong fibers, meaning that they can accumulate the micro-scale resistance forces exerted on each tiny segment of silk along the long length of fibers.

Table 1 Comparison of fluid dynamic and geometric characteristics of various shapes of an object according to flow conditions (see Eqns. (1) and (2); Hoerner 1965, Happel and Brenner 1986). 3D: three-dimensional geometry, 2D: two-dimensional geometry, 1D: one-dimensional geometry. (Cho 2020)

$$Cost \ efficiency = \frac{Acquired \ fluid \ dynamic \ force \ (or \ coefficient)}{Invested \ weight \ of \ a \ material \ (or \ volume)} \tag{6}$$

## The Significance of Multiple Ballooning Fibers

Here, it should be noted that the drag force of a fiber is less sensitive in respect to its diameter, while it is almost linearly proportional to its length. Because of this characteristic, it is more beneficial for spiders to spin thinner but longer or multiple ballooning fibers during their aerial locomotion. In order to prove this, two assumptions are considered: one is that a spider uses the limited (constant) amount of silk dope in order to spin ballooning fibers; the other is that the target drag force is constrained to be identical with a spider's body weight, 1-g (gravitational force equivalent) flight condition. The effect of fiber thickness is investigated under these two different assumptions.

In the case of material constraint, the question arises, what could be the best geometry to harvest fluid-dynamic forces of the air flow efficiently using certain amount of material? For spiders there are two alternatives, either spinning a single thick spider silk like a dragline or spinning multiple thin fibers. The total amount of silk dope,  $V_{silk\ dope}$ , used for the spinning of ballooning fibers can be described as in equation (7).

$$V_{silk\ dope} = \frac{\pi}{4} n d^2 L \tag{7}$$

The number of fibers varies according to the thickness of a fiber, the amount of silk dope being the same (see Eqn. (8)). As the thickness of a fiber decreases, the number of ballooning fibers is multiplied (see Eqn. (8)). This results in the increase of the drag force on the ballooning fibers (see Eqn. (11)). This relationship is shown in Figure 4A. Here, the drag force is expressed as a translational resistance coefficient, which is defined as  $K_T = F_T/\mu U$ 

(Happel and Brenner 1986). The tangential drag force of a fiber is considered in our analysis, because it describes a free-fall case in updraft wind. Fluid-dynamic interaction between fibers is not considered in the calculation.

It may be erroneously assumed that the drag of the ballooning fibers in low Reynolds-number flow is proportional to their wetted surface area, which is contact with the external airflow; however, as Figure 4B shows, the drag force of multiple ballooning fibers is more closely correlated with the number of fibers, not their wetted surface area of the ballooning fibers. The drag force on the ballooning fibers is proportional to  $1/d^2$  (see Eqn. (11)). The total wetted surface area of the ballooning fibers is proportional to 1/d (see Eqn. (10)). The number of ballooning fibers is proportional to  $1/d^2$  (see Eqn. (8)). Therefore, the number of fibers is a much more significant factor than their total surface area. This happens because, in relation to the drag force on a thin fiber, the existence of a fiber is important, but its thickness is not important.

$$n = \frac{4V_{silk\ dope}}{\pi d^2 L} \tag{8}$$

$$S_{wet} = n \left( \frac{\pi d^2}{2} + \pi dL \right) \cong \pi n dL \tag{9}$$

$$S_{wet} \cong \frac{4V_{silk dope}}{d} \tag{10}$$

$$S_{wet} \cong \frac{4V_{silk \, dope}}{d} \tag{10}$$

$$F_{T_{total}} = \frac{8\mu UV_{silk \, dope}}{d^2 \left[ ln \left( 2\frac{L}{d} \right) - 0.72 \right]} \tag{11}$$

Figure 4 (A) Translational resistance coefficient versus diameter of a ballooning fiber. The amount of silk dope is constrained as a constant value. The amount of silk dope is estimated using the average dimensions of observed ballooning fibers for a 20 mg crab spider (Cho et al. 2018). The length of ballooning fibers is kept at 3.22 m. (B) Triple y-axis chart for translational resistance coefficient, wetted surface area, and the number of ballooning fibers versus a reciprocal of a fiber diameter.

As the diameter of a ballooning fiber decreases, spiders can spin a greater number of fibers. This multiplication enlarges the drag force on the ballooning fibers. However, this miniaturization of thickness will not happen continually. The main constraint of the minimum thickness could be the ultimate tensile strength of a ballooning fiber. As the ballooning fiber becomes thinner, it can no longer endure the drag force on it. Considering this mechanical constraint, the material benefit of ballooning fibers according to their diameter is here investigated.

Factor of safety,  $S_f$ , is defined as the ratio of ultimate stress to actual stress,  $\frac{4W_{body}}{(\pi nd^2)}$ , which is under 1-g flight condition (see Eqn. (12)). The ultimate stress of a ballooning fiber, which is an aciniform gland silk, is 687 MPa (Hayashi et al. 2004, Cho et al. 2018). The values of a 20 mg *Xysticus* spp. ( $W_{body} = 196 \,\mu N$ , n = 60,  $d = 211 \,nm$ ) are used for the calculation (Cho et al. 2018). In the case of the crab spider, the factor of safety is calculated as 6.7.

$$S_f = \frac{\text{ultimate stress of a ballooning fiber}}{\text{actual stress on ballooning fibers}} = \frac{\pi n d^2 \sigma_u}{4W_{body}}$$
 (12)

1-g flight can be described by equating the spider's body weight and the fluid-dynamic force on its ballooning fibers (see Eqn. (13)). The length of a ballooning fiber in the air flow is constrained mechanically with respect to its diameter and flow velocity. By combining Eqns. (12) and (13), Eqn. (14) is derived, which permits the durable length of a ballooning fiber to be determined, considering the safety factor of 6.7. When the number of fibers is 1, n=1, the length of fiber is constrained for fluid-dynamic reasons to sustain 20 mg mass in the air (see Eqns. (13)), because the thickness of a fiber is large enough to bear a 20 mg weight. However, once the thickness of a fiber decreases, it cannot endure the fluid dynamic loads from a certain thickness. It should be shortened and the number of fibers should be multiplied to decrease the aerodynamic load and share the load to multiple fibers. In this case, the length of fibers and the number of fibers are constrained mechanically (see Eqn. (14) and Figure 5A). Eqn. (15) is derived by substituting Eqn. (8) into Eqn. (13). Figure 5B, which is drawn according to Eqn. (15), shows the silk dope required to sustain a 20 mg crab spider in the air according to fiber diameter. As spiders use thin and multiple ballooning fibers, spiders use the minimum amount of their silk dope for their aerial dispersal.

$$W_{body} = n \frac{2\pi\mu UL}{ln\left(2\frac{L}{d}\right) - 0.72} \tag{13}$$

$$\frac{\sigma_u}{S_f} = \frac{8\mu UL}{d^2 \left[ ln \left( 2\frac{L}{d} \right) - 0.72 \right]} \tag{14}$$

$$V_{silk\ dope} = \frac{W_{body} \left[ ln \left( 2\frac{L}{d} \right) - 0.72 \right] d^2}{8\mu U}$$
(15)

Figure 5 (A) Combination of length, thickness and the number of fibers to sustain the 20 mg weight of a crab spider. The blue dotted line indicates the average value of thicknesses of ballooning fibers in crab spiders. The red dash-dotted line is the average length of ballooning fibers of crab spiders (Cho et al. 2018). (B) The required amount of silk dope to sustain their bodies in the air (see Eqn. (15)). The blue dotted line indicates the average value of thicknesses of ballooning fibers in crab spiders. The red dash-dotted line presents the averaged total volume of silk dope used by crab spiders (Cho et al. 2018). The black dashed line shows the constant drag force on fibers because of the 1-g flight condition.

#### Nanoscale and the Rarefaction Effect of the Air

The nanoscale of ballooning silk raises the question of whether or not the continuity of the air is still valid on such a small-object scale. This is important, because it determines the validity of classical fluid dynamics applied to this problem. Air is different from liquid water, as it has more sparse molecules; this can be parameterized through a comparison to the mean free path of the molecules, which is defined as the average travel distance of a moving particle. While liquid water has a very small mean free path of 0.3 nm, the mean free path of the air is 65.44 nm (Jennings 1988, Marable et al. 2017). The ratio of the mean free path to the scale of an object is known as the Knudsen number ( $Kn = \lambda/D = 2\lambda/d$ ; the radius is the characteristic length in the case of fibrous structure; Brown 1993, Beskok et al. 2001, Zhao and Povitsky 2013, Zhao et al. 2016), determining whether or not the continuity of a medium is valid for their dynamics (Sun and Boyd 2004, Liu and Aono 2009, Santhanakrishnan et al. 2014; see Figure 6).

Figure 6 Comparative sketch of a ballooning fiber and the movement of air molecules. The thickness of a ballooning fiber is comparable to the mean free path of air molecules. The mean free path of air molecules, 65 nm, is approximately 22 times of their mean intermolecular distance, 3nm, (mean distance between particles). Therefore, actual distribution of air molecules is much denser than the distribution of air molecules, which is shown in the sketch. (Jennings 1988, Merodio and Saccomandi 2011, Marable et al. 2017)

The fluid states, both in micro-electro-mechanical systems (MEMS) and in the rarefied gas environment, can be categorized into four flows: (i) continuum; (ii) slip; (iii) transition; and (iv) free molecule flows (Karniadakis et al. 2005, Gad-el-Hak 2006, Pitakarnnop 2014). If Kn < 0.001, the flow is regarded as a continuum, such that the no-slip condition is validated on the surface of the object. For  $0.001 \le Kn < 0.1$ , it is still regarded as a continuum, but the slip boundary condition should be applied. The regime of Knudsen numbers  $0.1 \le Kn < 10$  is moderately rarefied. This regime is defined as the transition regime, in which the state changes from the continuum state to the highly rarefied state. Moreover, the regime of  $10 \le Kn$  is defined as the free molecule regime, in which the molecules can move relatively freely with decreased frequency of collisions with the object (Gad-el-Hak 2006, Tian et al. 2017). While most micro-swimmers in liquid and plumed aerial seeds in the air remain in the continuum or the near-slip regimes of the flow (the Knudsen number ranges from  $10^{-4}$  to  $10^{-2}$ ), a ballooning silk in the air and a DNA molecule in a liquid solution are categorised as part of the transition regime, as the Knudsen numbers of both are large, at 0.65 and 0.25, respectively (see

Table 2). Therefore, the rarefaction effect of the air should be investigated.

Table 2 Reynolds numbers and Knudsen numbers of various filament structures in nature. The thickness (diameter) of a filament structure is used as the characteristic length in the calculation of the Reynolds number. The radius of a filament structure is used for the calculation of the Knudsen number. (Cho 2020)

The correction of the Stokes drag of a spherical particle for the rarefaction of a fluid medium was established by Cunningham (1910) and Millikan (1923b). Later, the modelling of the influence of the transition regime on a non-spherical particle was developed by smoothing the resistance from the continuum to the free molecular regimes (Dahneke 1973b, Tian et al. 2017). The drag anisotropy is modeled by adjusting the diameter of the spherical particle, an "adjusted sphere" method. The Cunningham correction is applied to the drag of the non-spherical particle so as to introduce the effect of the slip condition (Dahneke 1973b, Tian et al. 2017). In this way, the anisotropic drag of the non-spherical particle in high Knudsen-number cases can be investigated. For the detailed

procedure, reference should be made to the correction procedure for the rarefied gas, established by Tian et al. (2017, see Appendix A in supplementary material). Figure 7A shows the variation of translational resistance coefficients of a 3.22 m-long circular cylinder as the thickness of the rod (fiber) varies. Figure 7B expresses the variation of the translational resistance coefficients according to Knudsen number. Both figures compare the theoretical and empirical values of drag coefficients of a fiber under the condition of low Reynolds-number flow with the theoretical values, which are corrected considering the rarefaction effect of air molecules as the thickness of a fiber decreases. The blue dotted line indicates the position of ballooning fibers that are observed in nature. The results are interesting: the drag coefficient, which considered the rarefaction effect of the air, begins to split at Kn = 0.065 from the values of the continuum-assumed drag coefficient and fall drastically after Kn = 0.65 (see Figure 7B). From this, it is suggested that the mean thickness of ballooning silk, 200 nm, may be the near region to lower boundary, where the continuum of the air is valid to its dynamics. Spider silks that were thinner (d < 100 nm); Kn > 1.3) cannot produce drag forces efficiently, not likely as it produce drag forces at a low Knudsen number (Kn < 1.3; d > 100 nm).

Figure 7 Rarefaction effect of air molecules on a fiber. (A) The translational resistance coefficient of a fiber 3.22 m long according to its diameter. (B) The translational resistance coefficient of a fiber 3.22 m long according to Knudsen number. The empty squares indicate theoretical values without consideration of the rarefaction effect (Eqns. (2) and (4)). The empty circles indicate empirical values without consideration of the rarefaction effect (Suter 1991). The solid squares are the theoretical values, with consideration of the rarefaction effect of air molecules. The rarefaction effect dominant region is marked with light yellow color. Light blue colors indicate the distributed region of crab spiders' ballooning fibers, 121–323 nm (Cho et al. 2018). The blue dotted line is the position of their averaged value, 211 nm.

It may be asked whether this proposition is plausible in the real world or not: the answer could come from studies in the air filter industry. Recently, an air filter consisting of fibrous structures was proposed and proven efficient experimentally by Zhao et al. (2016). A fiber diameter of 60–100 nm was determined to be the most effective for slip flow, which means that fiber diameters below 100 nm produce small drag force. This result strongly supports the proposition that a fiber diameter of approximately 200 nm is the minimum mean size for a fibrous structure that can effectively harvest aerodynamic force by producing drag.

Figure 8 shows summary of the all above discussed points. The variation of total drag force on the ballooning fibers of a 20 mg crab spider is plotted with respect to diameter of the fibers according to different vertical wind speeds. The rarefaction effect of the air molecules on the ballooning fibers is considered. (The fluctuation effect

of the air current on flexible fibers and interaction between fibers are not considered.) The cost efficiency of the fibers is superposed on the plot. As we see, the cost efficiency,  $\propto 1/d^2$ , increases according to decrease of fiber thickness. However, mechanical constraint exists because of the thinness of fibers. This establishes the lower boundary of the ballooning fibers. As we discussed above, we also observe the rapid drop of drag forces at the thickness below 100 nm. We thus ascertain that the thickness scale of ballooning fibers is located very near edge of these proposed boundaries.

Figure 8 Variation of drag force versus diameter of a ballooning fiber. The length and the number of fibers are kept constant upon the values of 20 mg crab spider, *Xysticus* spp. ( $L=3.22\ m,\ n=60$ ; see Eqn. (16)). The mechanical constraint is constructed by Eqn. (17). The cost efficiency is defined by Eqn. (18). The elliptic gray region represents the region of a 20 mg crab spider with 60 number of ballooning fibers in nature. The rectangular gray region indicates slip condition on the ballooning fibers because of the rarefaction effect of air molecules.

$$F_{T_{total}} = n \frac{2\pi\mu UL}{ln\left(2\frac{L}{d}\right) - 0.72} \tag{16}$$

$$F_u = \frac{\pi n d^2 \sigma_u}{4} \tag{17}$$

$$\eta_{cost} = \frac{K_T}{V_{silk}} = \frac{F_{T_{total}}}{\mu U V_{silk}} = \frac{8}{d^2 \left[ ln \left( 2\frac{L}{d} \right) - 0.72 \right]}$$
(18)

#### Conclusion

As spiders utilize a fiber structure for their passive flight, geometric and dimensional characteristics are explored from the viewpoint of fluid dynamics, using a mathematical fiber model. Dimensional investigation reveals that a filament structure is a materially efficient structure to produce fluid dynamic force in low Reynolds-number flows (Re < 1, viscous flow), while a membranous structure has advantages materially in moderate and high Reynolds-number flows (Re > 1000). Multiple thin fibers enable either maximizing their drag force under the

use of constant amount of silk material or minimizing the use of material to suspend a spider's body in the air. This is possible because of the interesting fluid-dynamic characteristics of a fiber in low Reynolds-number flow: the drag force of a fiber is less sensitive to variation of its diameter, while it is almost linearly proportional to its length. The thickness of a ballooning fiber, which ranges from 121 to 323 nm (average: 211 nm, N=40), allows for us to survey a rarefaction effect of air molecules, because these sizes are comparable to the mean free path of air molecules, 65.44 nm. The theoretical model proposes that 100 nm thickness is the lowest boundary of a fiber that can produce viscous drag force effectively. This is a reasonable result, because the most efficient (low drag) fibrous filter for slip flow (small drag) utilizes fibers of 60–100 nm thickness. It is recommended that future work should test the present hypothesis by investigating whether the thickness of ballooning fibers, which range from 121 to 323 nm, also appear in other species of ballooning spiders. Additionally, as it is recently observed that electric field elicits spiders' ballooning behavior, the study of geometric advantage of ballooning fibers in electric field would be also interesting future work.

#### **Acknowledgments**

The author thanks Klaus Affeld, Peter Neubauer, and Ingo Rechenberg for scientific discussions and support.

## **Funding**

This work was supported by the Elsa Neumann Scholarship (grant number T61004) and the German Academic Exchange Service (DAAD STIBET Degree Completion Grant, project number 10043380).

## List of symbols and abbreviation

а	radius of a sphere and a disk
Cc	Cunningham correction factor
$C_D$	drag coefficient
D	characteristic length
d	diameter of a fiber (the unit is meter in Suter's formula)
$d_{adj}$	adjusted diameter of a non-spherical particle

$d_{adj}$ $_{\perp}$	adjusted diameter of a non-spherical particle in the direction normal to the axis of the particle
$d_{adj}$ $\parallel$	adjusted diameter of a non-spherical particle in the direction parallel to the axis of the particle
$d_L$	characteristic length of the particle
F	fluid-dynamic force
$F_D$	fluid-dynamic force of a disk (normal to flow)
$F_{D,con}$	fluid-dynamic force in a continuum regime
$F_{D,tran}$	fluid-dynamic force in a transition regime
$F_N$	drag force in the direction normal to the axis of the cylinder (or a straight fiber)
$F_T$	drag force in the direction parallel to the axis of the cylinder (or a straight fiber)
$F_{T_{Suter}}$	drag force in the direction parallel to the axis of the cylinder (or a straight fiber) which is calculated from Suter's empirical formula (the unit is $\mu N$ )
$F_{T_{total}}$	total drag force on ballooning fibers in the direction parallel to the axis of the fibers
$F_u$	ultimate force
K	dynamic shape factor
Kn	Knudsen number
$K_T$	translational resistance coefficient, $K_T = F_T/\mu U$
L	length of a fiber (the unit is meter in Suter's formula)
N	the number of samples (or specimens)
n	the number of fibers
Re	Reynolds number
$R_N$	non-dimensional resistance coefficient in the direction normal to the axis of the cylinder (or a straight fiber)
$R_T$	non-dimensional resistance coefficient in the direction parallel to the axis of the cylinder (or a straight fiber)
$\mathcal{S}_f$	factor of safety
$S_{wet}$	wetted surface area of ballooning fibers
U	flow velocity (the unit is meter per second in Suter's formula); characteristic flow velocity
$V_{silk}$	total volume of ballooning fibers
$V_{silk\;dope}$	total volume of silk dope, that is used for spinning of ballooning fibers
$W_{body}$	weight of a spider body
$\alpha$	tangential momentum accommodation coefficient
β	slenderness of a non-spherical particle $(L/d)$
$\eta_{cost}$	volumetric cost efficiency for translational resistance coefficient
λ	mean free path
$\mu$	dynamic viscosity of fluid
ho	density of a fluid
$\sigma_u$	ultimate tensile stress of a material, $\sigma_u = F_u/A$ (A: cross sectional area)

#### References

Acharya T, Falgoust J, Schoegl I, Martin MJ. 2019. Measurement of Variation of Momentum Accommodation Coefficients with Molecular Mass and Structure. Journal of Thermophysics and Heat Transfer 33:773–78.

Agrawal A, Prabhu SV. 2008. Survey on measurement of tangential momentum accommodation coefficient. Journal of Vacuum Science & Technology A: Vacuum, Surfaces, and Films 26:634–45.

Alexander DE. 2015. On the wing New York: Oxford University Press.

Autumn K, Peattie AM. 2002. Mechanisms of adhesion in geckos. Integrative and comparative biology 42:1081–90.

Autumn K, Sitti M, Liang YA, Peattie AM, Hansen WR, Sponberg S, Kenny TW, Fearing R, Israelachvili JN, Full RJ. 2002. Evidence for van der Waals adhesion in gecko setae. Proceedings of the National Academy of Sciences of the United States of America 99:12252–56.

Barth FG, Komarek S, Humphrey JAC, Treidler B. 1991. Drop and swing dispersal behavior of a tropical wandering spider. J Comp Physiol A 169.

Beskok A. 2001. Validation of A New Velocity-Slip Model for Separated Gas Microflows. Numerical Heat Transfer, Part B: Fundamentals 40:451–71.

Blake J, Sleigh M (Eds.). 1975. Hydrodynamical Aspects of Ciliary Propulsion. Presented at the Proceedings of the symposium on swimming and flying in Nature, vol 2.

Bomphrey RJ, Nakata T, Phillips N, Walker SM. 2017. Smart wing rotation and trailing-edge vortices enable high frequency mosquito flight. Nature 544:92–95.

Brown RC. 1993. Air filtration. 1. ed. ed Oxford: Pergamon Press.

Burgers JM. 1938. In Second Report on Viscosity and Plasticity, Verhandelingen der Koninklijke Akademie van Wetenschappen, Afdeeling Natuurkunde: Wiskunde, natuurkunde, scheikunde, kristallenleer, sterrenkunde, weerkunde, en ingenieurswetenschappen Noord-Hollandsche Uitgevers-Maatschappij.

Burkman LJ. 2009. Characterization of Hyperactivated Motility by Human Spermatozoa During Capacitation. Archives of Andrology 13:153–65.

Casseau V, Croon G, Izzo D, Pandolfi C. 2015. Morphologic and Aerodynamic Considerations Regarding the Plumed Seeds of Tragopogon pratensis and Their Implications for Seed Dispersal. PloS one 10:e0125040.

Childress S. 1981. Mechanics of swimming and flying, Cambridge studies in mathematical biology Cambridge: Cambridge University Press.

Cho M, Neubauer P, Fahrenson C, Rechenberg I. 2018. An observational study of ballooning in large spiders: Nanoscale multifibers enable large spiders' soaring flight. PLoS biology 16:e2004405.

Cho M 2020. Suspension of a Point-Mass-Loaded Filament in Non-Uniform Flows: The Ballooning Flight of Spiders. Technical University of Berlin Repository

Cummins C, Seale M, Macente A, Certini D, Mastropaolo E, Viola IM, Nakayama N. 2018. A separated vortex ring underlies the flight of the dandelion. Nature 562:414–18.

Cunningham E. 1910. On the Velocity of Steady Fall of Spherical Particles through Fluid Medium. Proceedings of the Royal Society A: Mathematical, Physical and Engineering Sciences 83:357–65.

Dahneke BE. 1973a. Slip correction factors for nonspherical bodies—I Introduction and continuum flow. Journal of Aerosol Science 4:139–45.

Dahneke BE. 1973b. Slip correction factors for nonspherical bodies—II free molecule flow. Journal of Aerosol Science 4:147–61.

Darwin C. 1845. Journal of researches into the natural history and geology of the countries visited during the voyage of H.M.S. Beagle round the world, , under the Command of Capt. Fitz Roy, R.N. Second Edition. ed New York: John Murray, Albemarle Street.

Dudley R. 2002. The biomechanics of insect flight. 2. print., 1. paperback print. ed, Princeton paperbacks Princeton, NJ: Princeton Univ. Press.Ferrón HG, Botella H. 2017. Squamation and ecology of thelodonts. PloS one 12:e0172781.

Fan F-G, Ahmadi G. 2000. Wall Deposition of Small Ellipsoids from Turbulent Air Flows—A Brownian Dynamics Simulation. Journal of Aerosol Science 31:1205–29.

Ferrón HG, Botella H. 2017. Squamation and ecology of thelodonts. PloS one 12:e0172781.

Fung YC. 1990. Biomechanics New York, NY: Springer.

Gad-el-Hak M. 2006. The MEMS handbook. 2nd ed. ed, Mechanical engineering series Boca Raton, Fla.; London: CRC Taylor & Francis.

Glick PA. 1939. The distribution of insects, spiders, and mites in the air. USDA Tech Bull 1–150.

Gorham PW. 2013. Ballooning Spiders: The Case for Electrostatic Flight. arXiv.

Greene DF, Johnson EA. 1990. The Aerodynamics of Plumed Seeds. Functional Ecology 4:117.

Happel J, Brenner H. 1991. Low Reynolds number hydrodynamics. 5. printing. ed, Mechanics of fluids and transport processes Dordrecht: Kluwer Acad. Publ.

Hayashi CY, Blackledge TA, Lewis RV. 2004. Molecular and mechanical characterization of aciniform silk: uniformity of iterated sequence modules in a novel member of the spider silk fibroin gene family. Molecular biology and evolution 21:1950–59.

Hemadri V, Agrawal A, Bhandarkar UV. 2018. Determination of tangential momentum accommodation coefficient and slip coefficients for rarefied gas flow in a microchannel. Sādhanā 43:5.

Hoelzel AR (Ed.). 2009. Marine mammal biology. [Repr.]. ed Malden, Mass.: Blackwell Science.

Hoerner SF. 1992a. Fluid-dynamic drag. 2nd ed. ed Bakersfield: Hoerner Fluid Dynamics.

Humphrey JAC. 1987. Fluid mechanic constraints on spider ballooning. Oecologia 73:469–77.

Jennings SG. 1988. The mean free path in air. Journal of Aerosol Science 19:159–66.

Karniadakis G, Aluru N, Antman SS, Beskok A, Marsden JE, Sirovich L. 2005. Microflows and Nanoflows, Interdisciplinary Applied Mathematics New York, NY: Springer Science+Business Media Inc.

Lee VMJ, Kuntner M, Li D. 2015. Ballooning behavior in the golden orbweb spider Nephila pilipes (Araneae. Front Ecol Evol 3:e86780.

Lissaman PBS. 1983. Low-Reynolds-Number Airfoils. Annu Rev Fluid Mech 15:223–39.

Liu H, Aono H. 2009. Size effects on insect hovering aerodynamics: an integrated computational study. Bioinspiration & biomimetics 4:015002.

Mandelkern M, Elias JG, Eden D, Crothers DM. 1981. The dimensions of DNA in solution. Journal of Molecular Biology 152:153–61.

Marable DC, Shin S, Yousefzadi NA. 2017a. Investigation into the microscopic mechanisms influencing convective heat transfer of water flow in graphene nanochannels. International Journal of Heat and Mass Transfer 109:28–39.

Merodio J, Saccomandi G. 2011. Continuum mechanics, Encyclopedia of Life Support Systems Physical Sciences, Engineering and Technology Sources U.K.: EOLSS Publishers/UNESCO.

Millikan RA. 1923a. Coefficients of Slip in Gases and the Law of Reflection of Molecules from the Surfaces of Solids and Liquids. Phys Rev 21:217–38.

Millikan RA. 1923b. The General Law of Fall of a Small Spherical Body through a Gas, and its Bearing upon the Nature of Molecular Reflection from Surfaces. Phys Rev 22:1–23.

Minami S, Azuma A. 2003. Various flying modes of wind-dispersal seeds. Journal of Theoretical Biology 225:1–14.

Morley EL, Robert D. 2018. Electric Fields Elicit Ballooning in Spiders. Current biology: CB 28:2324-2330.e2.

Oeffner J, Lauder GV. 2012. The hydrodynamic function of shark skin and two biomimetic applications. The Journal of experimental biology 215:785–95.

Perkins T, Smith D, Larson R, Chu S. 1995. Stretching of a single tethered polymer in a uniform flow. Science 268:83–87.

Pitakarnnop J. 2014. Rarefied gas flow in pressure and vacuum measurements. ACTA IMEKO 3:60.

Purcell EM. 1977. Life at low Reynolds number. American Journal of Physics 45:3–11.

Sane SP. 2003. The aerodynamics of insect flight. Journal of Experimental Biology 206:4191–4208.

Santhanakrishnan A, Robinson AK, Jones S, Low AA, Gadi S, Hedrick TL, Miller LA. 2014. Clap and fling mechanism with interacting porous wings in tiny insect flight. The Journal of experimental biology 217:3898–3909.

Sheldon KS, Zhao L, Chuang A, Panayotova IN, Miller LA and B Lydia. 2017. Revisiting the Physics of Spider Ballooning. In: Layton AT, Miller LA, editors. Women in Mathematical Biology. Association for Women in Mathematics Series Cham: Springer International Publishing. p. 163–78.

Smith DJ, Gaffney EA, Blake JR, Kirkman-Brown JC. 2009. Human sperm accumulation near surfaces. J Fluid Mech 621:289.

Sudo S, Matsui N, Tsuyuki K, Yano T (Eds.). 2008. Morphological Design of Dandelion. Presented at the The XIth International Congress and Exposition. Orlando, Florida USA.

Sun Q, Boyd ID. 1999. Flat-plate aerodynamics at very low Reynolds number. J Fluid Mech 502:199-206.

Suter RB. 1991. Ballooning in spiders. Ethology Ecology & Evolution 3:13–25.

Suter RB. 1999. An Aerial Lottery: The Physics of Ballooning in a Chaotic Atmosphere. 1:281–93.

Tian L, Ahmadi G, Tu J. 2017. Mobility of nanofiber, nanorod, and straight-chain nanoparticles in gases. Aerosol Science and Technology 51:587–601.

Wang X, Clarke JA. 2015. The evolution of avian wing shape and previously unrecognized trends in covert feathering. Proceedings Biological sciences 282:20151935.

Weis-Fogh T. 1973. Quick Estimates of Flight Fitness in Hovering Animals, Including Novel Mechanisms for Lift Production. Journal of Experimental Biology 169–230.

Woolley DM. 2003. Motility of spermatozoa at surfaces. Reproduction 126:259-70.

Wu TY-T, Brokaw CJ, Brennen C. 1975. Swimming and Flying in Nature Boston, MA: Springer US.

Yamaguchi H, Hanawa T, Yamamoto O, Matsuda Y, Egami Y, Niimi T. 2011. Experimental measurement on tangential momentum accommodation coefficient in a single microtube. Microfluid Nanofluid 11:57–64.

Zhao L, Panayotova LN, Chuang A, Sheldon KS, Bourouiba L, Miller LA. 2017. Flying Spiders: Simulating and Modeling the Dynamics of Ballooning. In: Layton AT, Miller LA, editors. Women in Mathematical Biology. Association for Women in Mathematics Series Cham: Springer International Publishing. p. 179–210.

Zhao S, Povitsky A. 2013. Coupled continuum and molecular model of flow through fibrous filter. Physics of Fluids 25:112002.

Zhao X, Wang S, Yin X, Yu J, Ding B. 2016. Slip-Effect Functional Air Filter for Efficient Purification of PM2.5. Scientific reports 6:35472.

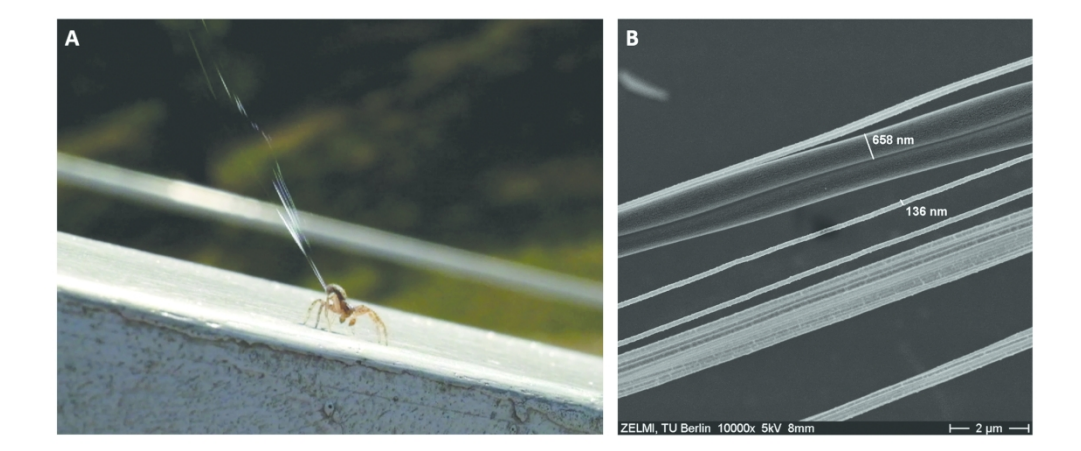


Figure 1 (A) A crab spider (Xysticus spp.) with ballooning fibers just before takeoff. (B) A picture of ballooning fibers by SEM ( $\times 10,000$ ). Two thick silks are the silks spun from minor ampullate silk glands. Multiples thin silks are aciniform silks. (Photos from Cho et al. 2018)

179x78mm (300 x 300 DPI)

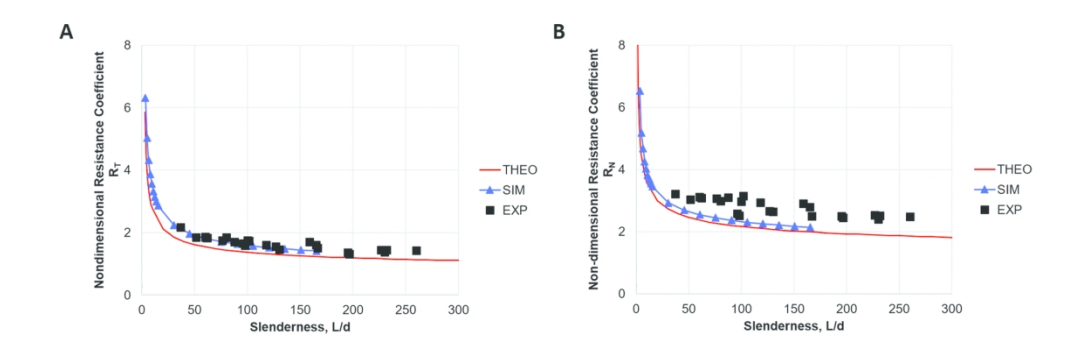


Figure 2 (A) Dimensionless longitudinal (tangential) resistance coefficients of a thin cylinder as a function of the slenderness of the cylinder. (B) Dimensionless transverse (normal) resistance coefficients of a thin cylinder as a function of the slenderness of the cylinder. The red solid lines are theoretical values. The triangular markers are the calculated values from the simulation using the bead-spring model. The square markers are the values obtained from the drop test (Cho 2020).

180x61mm (300 x 300 DPI)

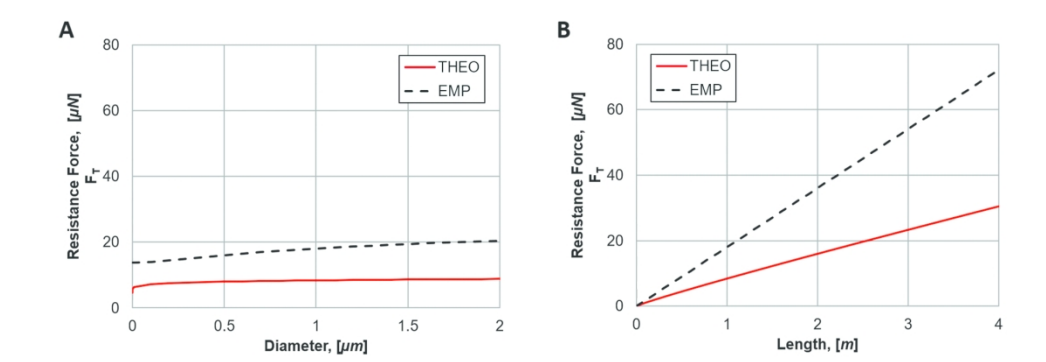


Figure 3 (A) The variation of resistance (drag) force on a thin fiber, which is 1 meter long, according to its diameter. The fluid medium is air. The flow velocity is 1 m/s. (B) The variation of resistance (drag) force on a thin fiber, the diameter of which is 1  $\mu$ m, according to its length. The fluid medium is air. The flow velocity is 1 m/s. The red solid lines are theoretical values with respect to equations (1) and (2). The black dashed lines are empirical values that are calculated by Suter's formula (see Eqn. (5); Suter 1991, Cho et al. 2018).

180x64mm (300 x 300 DPI)

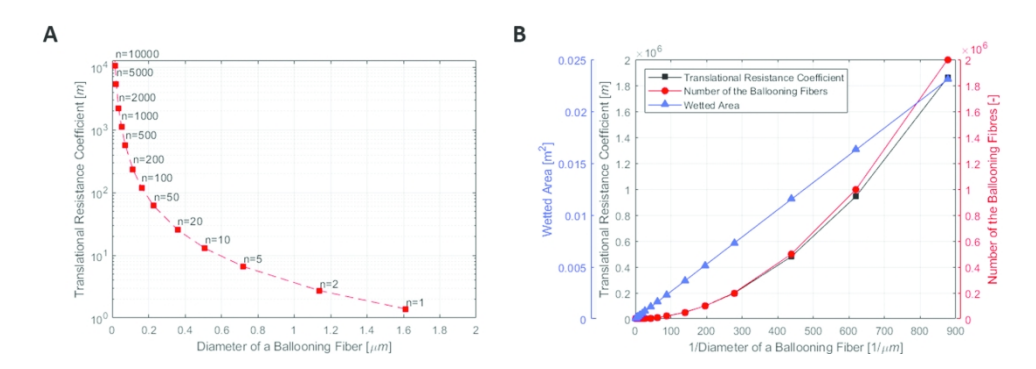


Figure 4 (A) Translational resistance coefficient versus diameter of a ballooning fiber. The amount of silk dope is constrained as a constant value. The amount of silk dope is estimated using the average dimensions of observed ballooning fibers for a 20 mg crab spider (Cho et al. 2018). The length of ballooning fibers is kept at 3.22 m. (B) Triple y-axis chart for translational resistance coefficient, wetted surface area, and the number of ballooning fibers versus a reciprocal of a fiber diameter.

180x61mm (300 x 300 DPI)

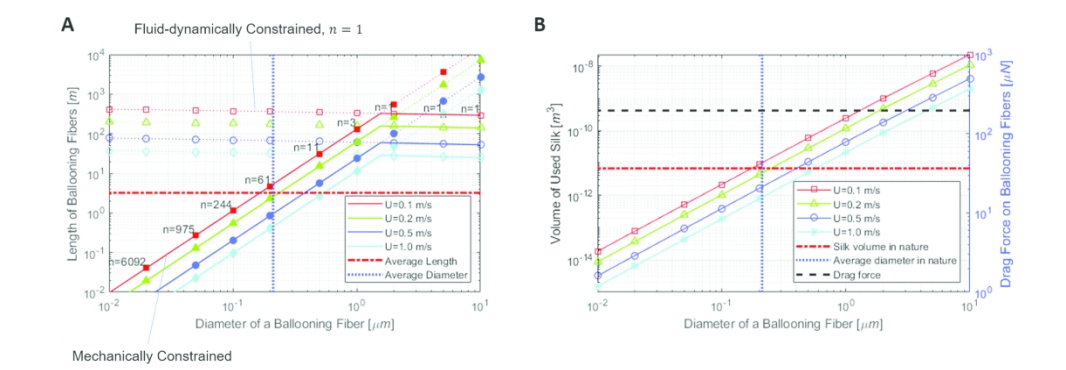


Figure 5 (A) Combination of length, thickness and the number of fibers to sustain the 20 mg weight of a crab spider. The blue dotted line indicates the average value of thicknesses of ballooning fibers in crab spiders. The red dash-dotted line is the average length of ballooning fibers of crab spiders (Cho et al. 2018). (B) The required amount of silk dope to sustain their bodies in the air (see Eqn. (15)). The blue dotted line indicates the average value of thicknesses of ballooning fibers in crab spiders. The red dash-dotted line presents the averaged total volume of silk dope used by crab spiders (Cho et al. 2018). The black dashed line shows the constant drag force on fibers because of the 1-q flight condition.

179x70mm (300 x 300 DPI)

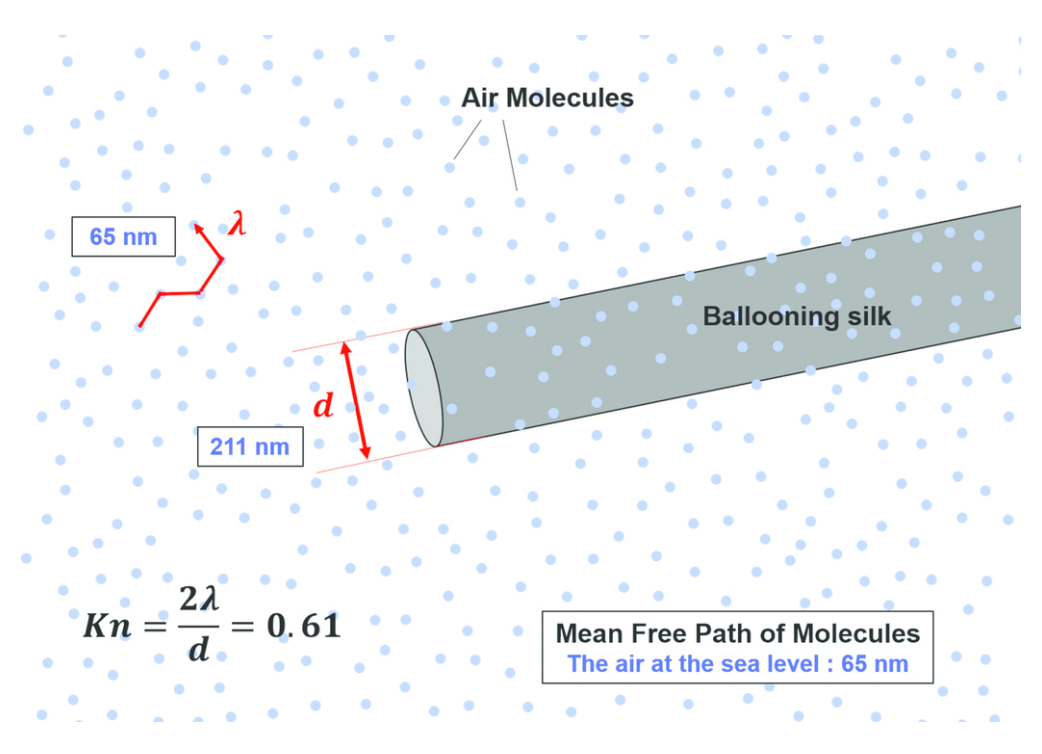


Figure 6 Comparative sketch of a ballooning fiber and the movement of air molecules. The thickness of a ballooning fiber is comparable to the mean free path of air molecules. The mean free path of air molecules, 65 nm, is approximately 22 times of their mean intermolecular distance, 3nm, (mean distance between particles). Therefore, actual distribution of air molecules is much denser than the distribution of air molecules, which is shown in the sketch. (Jennings 1988, Merodio and Saccomandi 2011, Marable et al. 2017)

87x60mm (300 x 300 DPI)

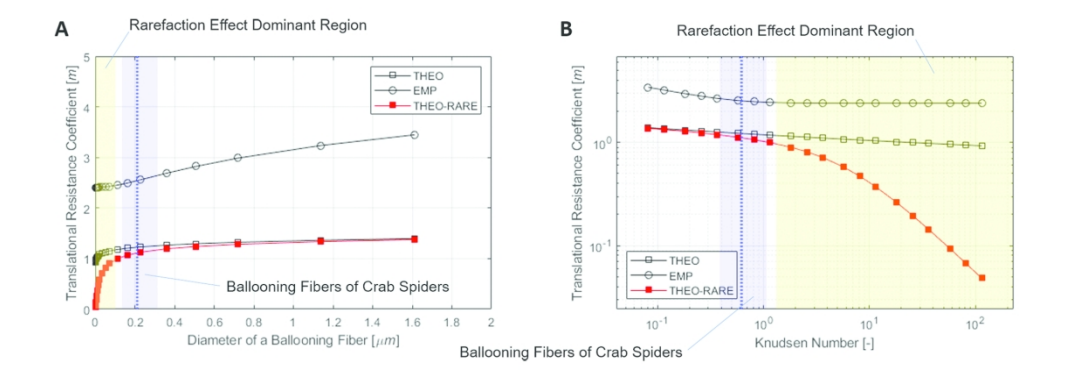


Figure 7 Rarefaction effect of air molecules on a fiber. (A) The translational resistance coefficient of a fiber 3.22 m long according to its diameter. (B) The translational resistance coefficient of a fiber 3.22 m long according to Knudsen number. The empty squares indicate theoretical values without consideration of the rarefaction effect (Eqns. (2) and (4)). The empty circles indicate empirical values without consideration of the rarefaction effect (Suter 1991). The solid squares are the theoretical values, with consideration of the rarefaction effect of air molecules. The rarefaction effect dominant region is marked with light yellow color. Light blue colors indicate the distributed region of crab spiders' ballooning fibers, 121–323 nm (Cho et al. 2018). The blue dotted line is the position of their averaged value, 211 nm.

180x65mm (300 x 300 DPI)

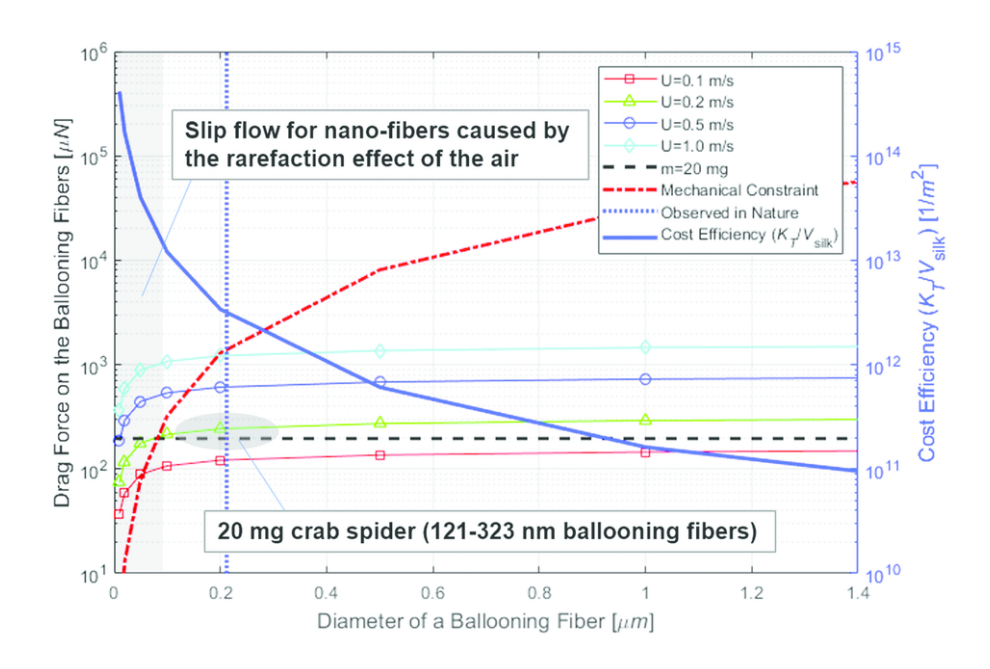


Figure 8 Variation of drag force versus diameter of a ballooning fiber. The length and the number of fibers are kept constant upon the values of 20 mg crab spider, Xysticus spp. (L=3.22 m, n=60; see Eqn. (16)). The mechanical constraint is constructed by Eqn. (17). The cost efficiency is defined by Eqn. (18). The elliptic gray region represents the region of a 20 mg crab spider with 60 number of ballooning fibers in nature. The rectangular gray region indicates slip condition on the ballooning fibers because of the rarefaction effect of air molecules.

87x60mm (300 x 300 DPI)

Flow Geometry		Drag Formula	Drag	Weight	Cost Efficiency (Drag/Weight)	
Re < 1	Sphere (3D)	$F = 6\pi\mu aU$	$\propto a \qquad \propto a^3$		$\propto \frac{1}{a^2}$	
Re < 1	Disk (2D)	$F_D = 16\mu aU$	$\propto \frac{1}{a}$			
Re < 1	Rod (1D)	$F_T = \frac{2\pi\mu UL}{\ln\left(2\frac{L}{d}\right) - 0.72}$	$F_T = \frac{2\pi\mu UL}{ln\left(2\frac{L}{d}\right) - 0.72} \qquad \qquad \propto L \qquad \qquad \propto L$			
Re > 1000	Sphere (3D)	$F = C_D \frac{1}{2} \rho U^2(\pi \alpha^2)$	$\propto a^2$	$\propto a^3$	$\propto \frac{1}{a}$	
Re > 1000	Disk (2D)	$F_D = C_D \frac{1}{2} \rho U^2(\pi \alpha^2)$	$\propto a^2$	$\propto a^2$	∝1	

	Spp.	Thickness	Length	Medium	Mean free path	Reynolds number	Knudsen number	Ref.
Ballooning silks	Xysticus	211 nm	3.22 m	Air	65.44 nm	0.002	0.654	Cho et al. 2018
Pappus	Dandelion Seed	15 μm	7 mm	Air	65.44 nm	0.258	$8.7 \times 10^{-3}$	Sudo et al. 2008
Stiff setae	Encarsia formosa	1.5 μm (1-2 μm)	20 μm	Air	65.44 nm	0.107	8.7 × 10 <sup>-2</sup>	Weis-Fogh 1973
Flagella	Sperm	1 μm	56 μm	Water ( ≈ Hydrated mucus)	~0.3 <sub>nm</sub>	0.00065	6 × 10 <sup>-4</sup>	Woolley 2003 Smith et al. 2009 Burkman 2009
Cilia	Paramecium	250 nm	12 μm	Water	~0.3 nm	0.00045	$2.4 \times 10^{-3}$	Blake and Sleigh 1975 Wu et al. 1975
DNA Molecule		2.4 nm (2.2-2.6 nm)	84 μm (the largest: 85 mm)	Concentrated polymer solution	~0.3 <sub>nm</sub>	6.6 × 10 <sup>-8</sup>	0.25	Mandelkern et al. 198 Perkins et al. 1995

Mean free path: data source Jennings 1988, Marable et al. 2017.

## **Supplementary Material**

#### Appendix A

## Calculation of Anisotropic Particle Drag in the High Knudsen Number Flows

While the drag of a spherical particle is well understood in the wide range of the Knudsen number flow, the drag of an isotropic particle (non-spherical particle) is not well studied. Recently, Tian et al. showed systematic description of that (2017). The rarefaction effect of the air on the nanoscale filament is investigated based on the methodology for a long cylinder. Here, the methodologies are introduced.

#### i. Continuum Regime

Drag force of a non-spherical particle in the low-Reynolds number and low Knudsen number flows is described as (A. 1).  $d_L$  is characteristic length of the particle. K refers as a dynamic shape factor and represent the characteristics of its geometry (Tian et al. 2017).

$$F_{D,con} = 3\pi\mu U d_L K \tag{A. 1}$$

The dynamic shape factor for a long cylinder is as follow (Burgers 1938):

$$K_{\parallel} = \frac{2\beta}{3[\ln(2\beta) - 0.72]}$$
 (A. 2)

#### ii. Free Molecular Regime

The shape factor for a long cylinder in the free molecular regime is as follow (Dahneke 1973a, Tain et al. 2017):

$$K'_{\parallel} = \frac{1}{Kn} \left[ \left( 2\beta + \frac{\pi}{2} - 2 \right) \alpha + 4 \right]$$
 (A. 3)

#### iii. Transition Regime

The formulation of the transition regime drag for a non-spherical particle is enabled by employing Cunningham correction which has been used for a sphere (Dahneke 1973b). This description well expresses the drag forces of a non-spherical particle in the continuum flow regime and the free molecular regime and also the smooth transition between both flow regimes. The anisotropic effect of a non-spherical particle in the transition regime is expressed by introducing "adjusted sphere" method and varying its diameter (Tian et al. 2017). The Eqns. (A. 4)-(A. 11) show the transition regime drag for a non-spherical particle (Fan and Ahmadi 2000).

$$F_{D,tran} = \frac{F_{D,con}}{Cc(d_{adj})} = \frac{3\pi\mu U d_L K}{Cc(d_{adj})}$$
(A. 4)

$$Cc(d_{adj}) = 1 + \frac{d_L}{d_{adj}} Kn \left( 1.257 + 0.4e^{\frac{-1.1d_{adj}}{Kn d_L}} \right)$$
 (A. 5)

$$d_{adj\perp} = \frac{1.657d_L\beta}{16(\beta^2 - 1)}(A \cdot B)$$
 (A. 6)

$$d_{adj \parallel} = \frac{1.657 d_L \beta}{8(\beta^2 - 1)} (C \cdot D)$$
 (A. 7)

$$A = \frac{2\beta^2 - 3}{\sqrt{\beta^2 - 1}} \ln\left(\beta + \sqrt{\beta^2 - 1}\right) + \beta \tag{A. 8}$$

$$B = E_p \left[ 4 + \left( \frac{\pi}{2} - 1 \right) \alpha \right] + \frac{G_p}{F_p^2} \left( 2 + \frac{4F_p^2 + \pi - 6}{4} \right) \alpha \tag{A. 9}$$

$$C = \frac{2\beta^2 - 1}{\sqrt{\beta^2 - 1}} \ln \left( \beta + \sqrt{\beta^2 - 1} \right) - \beta$$
 (A. 10)

$$D = 2E_p \alpha + \frac{G_p}{F_p^2} \left[ F_p^2 (4 - 2\alpha) - 4 + \left( 3 - \frac{\pi}{2\beta^2} \right) \alpha \right]$$
 (A. 11)

Tangential momentum accommodation coefficient (TMAC) is used as a particle momentum accommodation coefficient. The TMAC of the air on flat surface differs according to materials of the surfaces. The value ranges from 0.71 to 0.9 (Acharya et al. 2019). It is regarded that the roughness of the material is related to this variation. The value of 0.8 is used in order to investigate the rarefaction effect of the air on the ballooning fibres among different estimated and measured values (Millikan 1923a, Dahneke 1973a, Karniadakis et al. 2005, Agrawal and

Prabhu 2008, Yamaguchi et al. 2011, Hemadri et al. 2018, Acharya et al. 2019).